JACS
JOURNAL OF THE AMERICAN CHEMICAL SOCIETY
Article
pubs.acs.org/JACS

Lock-Arm Supramolecular Ordering: A Molecular Construction Set for Cocrystallizing Organic Charge Transfer Complexes

Anthea K. Blackburn,[†,#] Andrew C.-H. Sue,[†,#] Alexander K. Shveyd,[†] Dennis Cao,[†] Alok Tayi,[‡] Ashwin Narayanan,[‡] Brian S. Rolczynski,[†] Jodi M. Szarko,[†] Ozgur A. Bozdemir,[†] Rie Wakabayashi,[†] Jessica A. Lehrman,[†] Bart Kahr,[∥] Lin X. Chen,[†] Majed S. Nassar,[⊥] Samuel I. Stupp,*[,†,‡,§] and J. Fraser Stoddart*[,†]

[†]Department of Chemistry and [‡]Department of Materials Science and Engineering, Northwestern University, Evanston, Illinois 60208, United States

[§]Department of Medicine and Simpson-Querrey Institute for BioNanotechnology, Northwestern University, Chicago, Illinois 60611, United States

[∥]Department of Chemistry and Molecular Design Institute, New York University, New York, New York 10003, United States

[⊥]Joint Center of Excellence in Integrated Nanosystems, King Abdulaziz City for Science and Technology (KACST), Riyadh 11442, Kingdom of Saudi Arabia

Supporting Information

ABSTRACT: Organic charge transfer cocrystals are inexpensive, modular, and solution-processable materials that are able, in some instances, to exhibit properties such as optical nonlinearity, (semi)conductivity, ferroelectricity, and magnetism. Although the properties of these cocrystals have been investigated for decades, the principal challenge that researchers face currently is to devise an efficient approach which allows for the growth of high-quality crystalline materials, in anticipation of a host of different technological applications. The research reported here introduces an innovative design, termed LASO—lock-arm supramolecular ordering—in the form of a modular approach for the development of responsive organic cocrystals. The strategy relies on the use of aromatic electronic donor and acceptor building blocks, carrying complementary rigid and flexible arms, capable of forming hydrogen bonds to amplify the cocrystallization processes. The cooperativity of charge transfer and hydrogen-bonding interactions between the building blocks leads to binary cocrystals that have alternating donors and acceptors extending in one and two dimensions sustained by an intricate network of hydrogen bonds. A variety of air-stable, mechanically robust, centimeter-long, organic charge transfer cocrystals have been grown by liquid−liquid diffusion under ambient conditions inside 72 h. These cocrystals are of considerable interest because of their remarkable size and stability and the promise they hold when it comes to fabricating the next generation of innovative electronic and photonic devices.

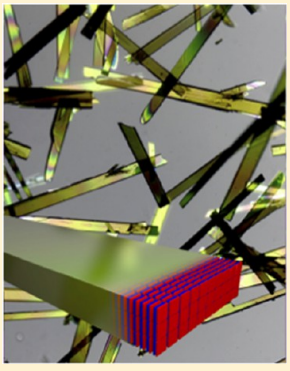

INTRODUCTION

It is often the case in supramolecular chemistry[1] that serendipity[2] plays a crucial role in defining new pathways in research. Such was the case in this research, where some time ago we set out to make a [2]catenane and stumbled upon a simple solid-state superstructure that expressed emergent behavior[3] on the centimeter scale at the supramolecular level. A seemingly straightforward approach to making a mechanically interlocked compound turned into an investigation of a new range of organic materials, which we were to discover[3] exhibit room-temperature ferroelectric hysteresis. We could not have predicted that the solid-state superstructure that emerges during the cocrystallization of two simple organic compounds, containing aromatic donors and acceptors carrying hydrogen bond acceptors and donors, would result—through charge transfer (CT) interactions—in a crystalline and infinite one-dimensional stack that displays complex behavior.[4] Such is the wonder of emergent phenomena,[5] which are observed when a number of components come together en masse to form a well-ordered array[6] with unexpected and useful properties. This progression from a serendipitous discovery involving the assembly through molecular recognition of simple building blocks is one of many examples[7] of setting out to accomplish one task in chemistry and finding oneself addressing another completely different goal in materials science.

Charge transfer (CT) interactions[8] constitute weak noncovalent bonding forces that have been well-explored since the middle of the last century in the context of emergent phenomena,[5] insofar as the organic complexes formed as a result of these interactions have been investigated for their structural modularity[9] and valuable properties.[10] CT interactions—specifically weak noncovalent attractions between electron-rich donors (D) and electron-deficient acceptors (A)—are generated from an electronic transition[11] leading to partial electron sharing (ρ) between the D−A molecules ($D^{+\rho}$–$A^{-\rho}$, $0 \leq \rho \leq 1$).

Received: September 15, 2014
Published: November 4, 2014

   dx.doi.org/10.1021/ja509442t | J. Am. Chem. Soc. 2014, 136, 17224−17235

The excitation energy of this resonance usually occurs in the visible spectrum, and the broad optical absorption bands observed in the UV−visible spectrum are referred to as CT bands.

In the solid state, aromatic D−A molecular complexes tend to cocrystallize via CT interactions in two different binary packing motifs—namely, segregated stacks[10,12] and mixed stacks.[10,13] In segregated stacks, the donors, D, and acceptors, A, stack in separate columns (···DDD···, ···AAA···) as a consequence of CT interactions, while in mixed stacks the donors, D, and acceptors, A, occupy alternating positions (···DAD···, ···ADA···) along the $\pi-\pi$ stacking direction. These two coconformations[14] exhibit very different emergent physical properties.[5] Segregated stacks, such as the cocrystal of tetrathiafulvalene-7,7,8,8-tetracyanoquinodimethane (TTF-TCNQ), exhibit[10,15] metallic conductivity, since the overlapping π orbitals between stacks of open-shell donors and acceptors merge into conduction bands. On the other hand, the mixed-stack systems are primarily dielectric materials and semiconductors and are known for their ferroelectric[3,16,17] and ambipolar change transport[18] properties, respectively. Other emergent physical properties,[5] including magnetic ordering[17,19] and optical nonlinearity,[20] have also been identified in mixed-stack CT cocrystals.

Given these emergent physical properties,[5] one of the major challenges when it comes to introducing CT cocrystals into technological settings is the production of high-quality, air-stable, single-crystalline materials of appropriate sizes. Inspired by the advances made with regard to supramolecular D−A assemblies[21] in solution, we report here a "lock-arm supramolecular ordering" (LASO) design strategy which takes advantage of the synergy among (i) CT interactions, (ii) hydrogen bonding, and (iii) solvophobic effects to produce *ordered, close-packed, solvent-free, and robust CT mixed-stack cocrystals on a centimeter-length scale*.

RESULTS AND DISCUSSION

Nine different CT cocrystals were obtained (Figure 1) as a result of the mixing and matching of 12 available building blocks, which were divided into 4 groups based on their electronic and hydrogen-bonding complementarity. Single crystals suitable for investigation by X-ray crystallography were obtained using a liquid−liquid diffusion protocol (see the Experimental Section). It is noteworthy that the cocrystals obtained and illustrated in this work are stable in air and remain crystalline even after their complete desolvation. These properties reveal not only the rigidity of the LASO network but also the promise that these cocrystals have in finding real-world applications. The cocrystallization conditions and X-ray structural data are summarized in the Experimental Section.

The LASO design element consists of three major components: (i) complementary aromatic *donor−acceptor cores*, (ii) complementary *hydrogen-bonding recognition units*—flexible diethylene glycol (DEG) arms and functional groups (carbonyl, amino, imide, and hydroxyl) capable of participating in intermolecular hydrogen-bonding interactions, and (iii) *solvophobic forces*, which promote the self-assembly/cocrystallization processes. It is noteworthy that the LASO strategy employs intrinsically flexible building blocks in concert with flat and rigid π-synthons in order to achieve molecular recognition involving orthogonal motifs. The dynamic stereochemical characteristics of the DEG arms—that is,

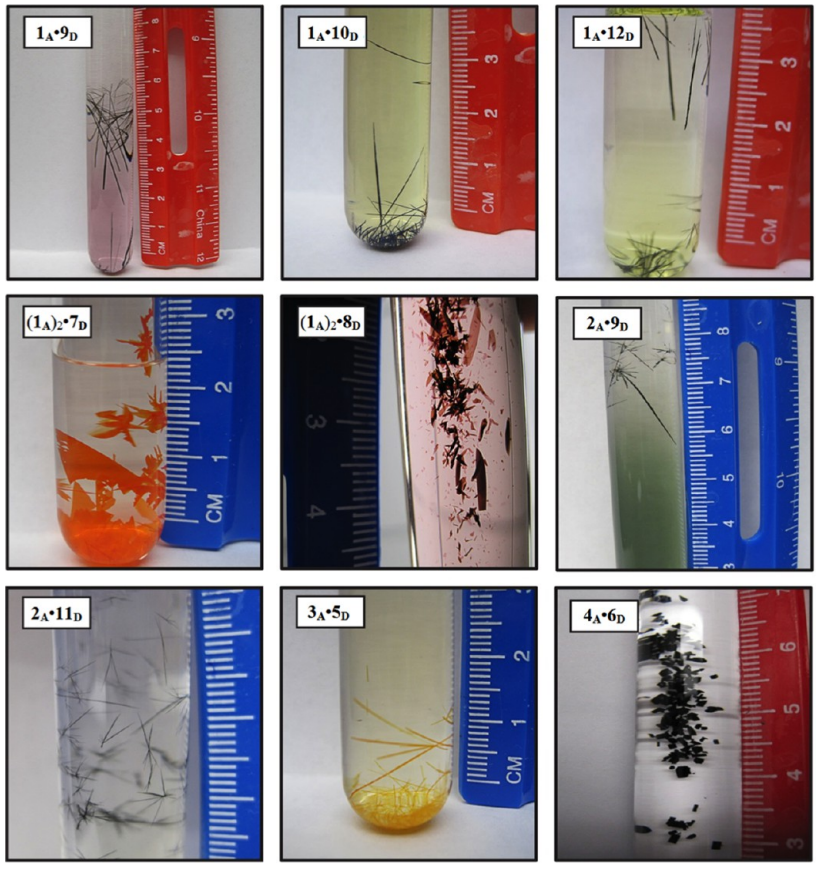

Figure 1. Photographic images of nine LASO cocrystals grown by the liquid−liquid diffusion protocol. The images were taken after 3−5 days of crystal growth.

dx.doi.org/10.1021/ja509442t | J. Am. Chem. Soc. 2014, 136, 17224−17235

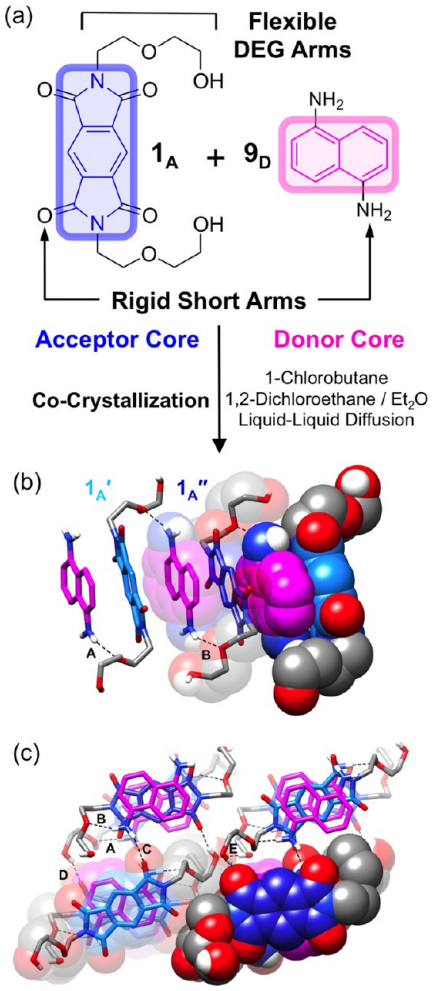

Figure 2. (a) Cocrystallization of pyromellitic diimide derivative acceptor $\mathbf{1}_A$ and 1,5-diaminonaphthalene donor $\mathbf{9}_D$ by liquid–liquid diffusion to form a LASO complex. (b) Intermolecular recognition units in the cocrystal $\mathbf{1}_A{\cdot}\mathbf{9}_D$ that participate in donor–acceptor interactions shown in magenta and blue, respectively, within a blend of tubular and space-filling representations of the solid-state superstructure of $\mathbf{1}_A{\cdot}\mathbf{9}_D$. Two conformational isomers of $\mathbf{1}_A$ are present in the cocrystal, labeled as $\mathbf{1}_A'$and $\mathbf{1}_A''$. The hydrogen-bonding interactions are depicted by black dashed lines, where the [N···O] hydrogen-bonding distances are found to be (A) 3.08 and (B) 3.23 Å for $\mathbf{1}_A'$ and $\mathbf{1}_A''$, respectively. (c) Superstructure of cocrystal $\mathbf{1}_A{\cdot}\mathbf{9}_D$ which contains further hydrogen-bonding interactions in addition to those identified as **A** and **B** revealed as a blend of tubular and space-filling representations of the solid-state superstructures of $\mathbf{1}_A{\cdot}\mathbf{9}_D$. The interstack [N···O] hydrogen-bonding distance is (C) 3.00 Å, and the [O···O] hydrogen-bonding distances are (D) 2.76 and (E) 2.82 Å. Aromatic and alkyl H atoms not participating in hydrogen-bonding interactions shown in this illustration are omitted for the sake of clarity. Color code: $\mathbf{1}_A$ PmI core, medium blue and light blue; $\mathbf{9}_D$ naphthalene core, magenta; C, gray; H, white; O, red; N, blue.

their predisposition to adopt[22] an ensemble of conformations and coconformations—facilitates the hydrogen-bonding interactions between the complementary D–A components during the cocrystallization processes. While the propensity for hydrogen bonding is engineered into the supramolecular design, the specific hydrogen-bonding patterns in the superstructures cannot be programmed or predicted from first principles—that is, the hydrogen-bonded networks adopted in the LASO CT cocrystals are not designed de novo but instead arise as a result of the molecular components engaging spontaneously in the most energetically favorable coconformations[21] in the solid state. The packing forces intrinsic to the cocrystals harness the conformational flexibility of the DEG arms to achieve intermolecular binding under coconformational[14] control in the lattice. This orthogonal source of molecular recognition distinguishes LASO complexes from other extended (super)structures utilizing rigid aromatic building blocks: e.g., coordination polymers[23] and metal–organic frameworks.[24]

Three groups of LASO cocrystals, which differ in the positions of the DEG arms on the aromatic cores, are presented in this full paper. Groups 1 and 2 have these DEG arms located on the electron-accepting aromatic core, while group 3 has these arms located on the electron-donating aromatic core. As will be shown, these subtle differences in structure can have a dramatic effect on the nature of the LASO cocrystals that form.

LASO Cocrystals in Group 1. The cocrystallization of the pyromellitic diimide (PmI) acceptor $\mathbf{1}_A$[3] and the 1,5-diaminonaphthalene donor $\mathbf{9}_D$ is illustrated in Figure 2. Liquid–liquid diffusion of 1-chlorobutane into a mixture of the D–A components in 1,2-dichloroethane and Et_2O yielded small cocrystals within a few hours, indicating the efficiency of the self-assembly process. A close examination of the superstructure[25,26] of cocrystal $\mathbf{1}_A{\cdot}\mathbf{9}_D$, which crystallized (Figures 3b,c) in the triclinic space group $P\bar{1}$, with two halves of a $\mathbf{1}_A$ molecule and one $\mathbf{9}_D$ molecule present in the asymmetric unit, reveals that acceptor $\mathbf{1}_A$ adopts two conformations (labeled $\mathbf{1}_A'$ and $\mathbf{1}_A''$) in the mixed stacks. The π–π interplanar separations between $\mathbf{9}_D$ and $\mathbf{1}_A'/\mathbf{1}_A''$ are consistent with those expected for the D–A interactions present and are found to be 3.47/3.32 Å, respectively. These alternating D–A stacks are further reinforced by both intra- and interstack hydrogen bonds between (i) the amino functions of $\mathbf{9}_D$ with the carbonyl groups of $\mathbf{1}_A$ ([N···O] distance 3.00 Å), (ii) the amino functions of $\mathbf{9}_D$ with the DEG arms of $\mathbf{1}_A$ ([N···O] distances 3.08 and 3.23 Å) and (iii) the DEG arms of $\mathbf{1}_A'/\mathbf{1}_A''$ ([O···O] distances 2.76/2.82 Å). As a result, the cocrystalline stacks are perfectly aligned so as to form an intricate three-dimensional network, where the D–A supramolecular components are tightly packed in the lattice and the cocrystal is completely devoid of any solvent molecules.

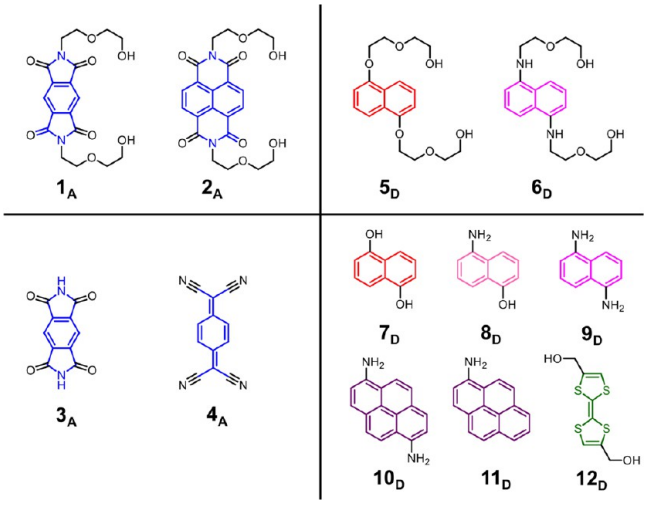

In addition to forming a cocrystal with $\mathbf{9}_D$, the PmI derivative $\mathbf{1}_A$, with flexible DEG arms, can serve as a promiscuous acceptor component in combination[27] with the donors $\mathbf{10}_D$ and $\mathbf{12}_D$. Superstructures of cocrystals $\mathbf{1}_A{\cdot}\mathbf{10}_D$[1] and $\mathbf{1}_A{\cdot}\mathbf{12}_D$,[3,28] which both crystallized in the monoclinic space group[25] $P2_1/c$ with half a

dx.doi.org/10.1021/ja509442t | J. Am. Chem. Soc. 2014, 136, 17224–17235

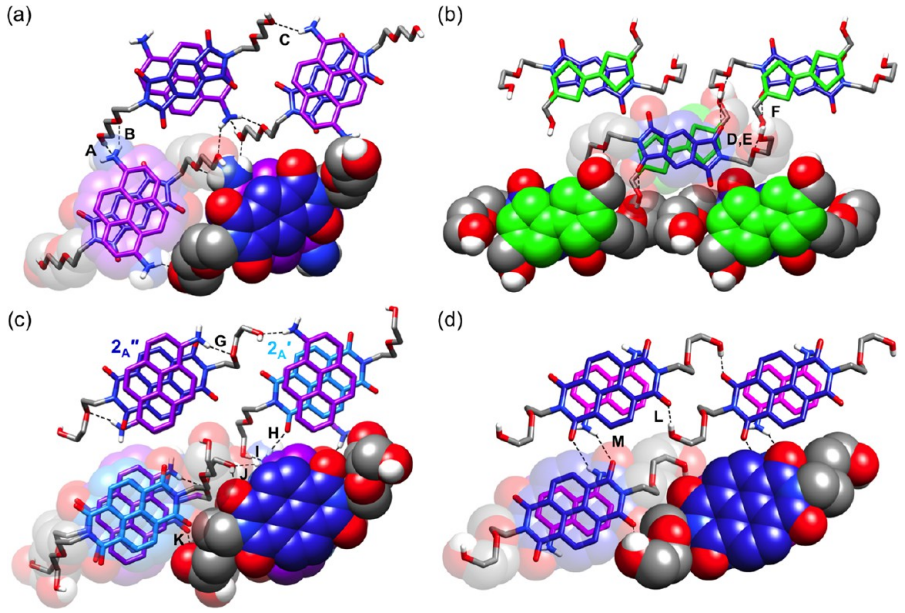

Figure 3. Solid-state superstructures, illustrated as a blend of tubular and space-filling representations, of LASO cocrystals (a) $\mathbf{1}_A\cdot\mathbf{10}_D$, (b) $\mathbf{1}_A\cdot\mathbf{12}_D$, (c) $\mathbf{2}_A\cdot\mathbf{11}_D$, and (d) $\mathbf{2}_A\cdot\mathbf{9}_D$, that form D−A mixed stacks, in which the acceptor components contain the flexible DEG arms and the donor components carry only rigid short arms. Hydrogen bonds are depicted by black dashed lines. (a) The amino functions of $\mathbf{10}_D$ participate in interstack hydrogen-bonding interactions with neighboring $\mathbf{1}_A$ molecules, where the [N···O] hydrogen-bonding distances are (A) 2.94, (B) 3.04, and (C) 2.96 Å. (b) The distances of three interstack [O···O] hydrogen-bonding interactions in cocrystal $\mathbf{1}_A\cdot\mathbf{12}_D$ are (D) 2.77, (E) 2.84, and (F) 3.41 Å. (c) In cocrystal $\mathbf{2}_A\cdot\mathbf{11}_D$, the interstack [N···O] hydrogen-bonding distances are (G) 3.17, (H) 3.01, (I) 2.85, and (J) 3.02 Å. The [O···O] hydrogen-bonding distance is (K) 2.82 Å. (d) Cocrystal $\mathbf{2}_A\cdot\mathbf{9}_D$ contains [N···O] hydrogen bonds with distances of (L) 2.82 and (M) 3.49 Å, respectively. Aromatic and alkyl H atoms, not participating in hydrogen-bonding interactions shown in this illustration, are omitted for the sake of clarity. Color code: $\mathbf{1}_A$ PmI core, medium blue; $\mathbf{2}_A$ NDI core, light and medium blue; $\mathbf{9}_D$ naphthalene core, magenta; $\mathbf{10}_D$ and $\mathbf{11}_D$ pyrene core, purple; $\mathbf{12}_D$ TTF core, green; C, gray; H, white; O, red; N, blue.

donor molecule and half an acceptor molecule in the asymmetric unit, are illustrated in Figure 3a,b. It is interesting to note that the conformation of $\mathbf{1}_A$ and the overall hydrogen-bonding pattern change considerably when different donor partners are incorporated into the lattices. In contrast to the case for $\mathbf{1}_A\cdot\mathbf{9}_D$, cocrystal $\mathbf{1}_A\cdot\mathbf{10}_D$ contains only one conformation of the acceptor molecule, and the aromatic units are separated by a $\pi-\pi$ interplanar distance of 3.36 Å. Furthermore, in accordance with the LASO guidelines, a number of hydrogen-bonding interactions are observed in the cocrystal. Surprisingly, no intrastack hydrogen bonds are observed along the D−A stack between the amino functions of $\mathbf{10}_D$ and the DEG arms of $\mathbf{1}_A$. Instead, [C−H···O] bonding interactions between the DEG arms and the pyrene moiety are observed ([C···O] distance 3.44 Å). As expected, interstack hydrogen-bonding interactions are present between the $\mathbf{10}_D$ amino functions and the DEG arms of $\mathbf{1}_A$ molecules ([O···N] distances 2.94, 2.96, and 3.04 Å), as well as interstack [O−H···O] interactions between DEG arms of $\mathbf{1}_A$ molecules ([O···O] distance 3.29 Å). As a result of these interstack hydrogen-bonding interactions, stacks of $\mathbf{1}_A\cdot\mathbf{10}_D$ pack in a herringbone fashion. Similarly, the mixed stacks in cocrystal $\mathbf{1}_A\cdot\mathbf{12}_D$ have the $\mathbf{1}_A$ and $\mathbf{12}_D$ components separated by a $\pi-\pi$ interplanar distance of 3.36 Å. Although there are no intrastack hydrogen-bonding interactions present in the cocrystal, a multitude of interstack [O−H···O] interactions are present between the $\mathbf{12}_D$ hydroxyl groups and the $\mathbf{1}_A$ DEG arms which act to hold the stacks together in offset layers ([O···O] distances 2.77, 2.84, and 3.41 Å).

In addition to these three cocrystals, two further D−A pairs were employed as control experiments in order to demonstrate that the complementarity of the long DEG arms and the short functional groups is crucial to the growth of LASO cocrystals. These experiments involved the use of (i) the PmI acceptor $\mathbf{3}_A$, in which the DEG chains in $\mathbf{1}_A$ have been omitted, and the donor $\mathbf{9}_D$, as well as (ii) the PmI acceptor $\mathbf{1}_A$ and TTF, in which the diol functionality of $\mathbf{12}_D$ is omitted. Both control experiments failed to yield high-quality single cocrystals suitable for X-ray crystallography under the same conditions as those employed to grow cocrystals of $\mathbf{1}_A\cdot\mathbf{9}_D$ and $\mathbf{1}_A\cdot\mathbf{12}_D$. These control experiments underline the importance of the hydrogen-bonding network in obtaining LASO cocrystals.

The superstructures of two cocrystals containing the NDI-based acceptor $\mathbf{2}_A$[29] are illustrated in Figure 3c,d, both of which crystallized in the triclinic space group $P\bar{1}$ with one acceptor and one donor molecule in the asymmetric unit. Cocrystal $\mathbf{2}_A\cdot\mathbf{11}_D$ contains (Figure 3c) two types of symmetrically nonequivalent NDI acceptors (labeled $\mathbf{2}_A'/\mathbf{2}_A''$) aligned alternately in the one-dimensional mixed stacks which are separated by $\pi-\pi$ distances of 3.33 and 3.35 Å, respectively, from the $\mathbf{11}_D$ molecules they envelop. On account of the dissymmetrical structure of $\mathbf{11}_D$, the amino functions on the pyrene donor are disordered in an approximate 6:1 ratio across two positions throughout the superstructure. Intrastack hydrogen-bonding interactions are present between the $\mathbf{11}_D$ amino functions and the DEG arms of $\mathbf{2}_A$ ([N···O] distance 3.01 Å), as well as a wide variety of interstack interactions between the $\mathbf{11}_D$ amino functions in both its positions with the $\mathbf{2}_A$ DEG arms and between the DEG arms in neighboring cocrystal stacks ([N···O] distances 3.17, 3.02, and 2.85 Å; [O···O] distance 2.82 Å). These interactions hold the cocrystal stacks in slightly offset layers.

Cocrystal $\mathbf{2}_A\cdot\mathbf{9}_D$ consists (Figure 3d) of one-dimensional mixed stacks, in which the D and A molecules are separated by a

dx.doi.org/10.1021/ja509442t | J. Am. Chem. Soc. 2014, 136, 17224−17235

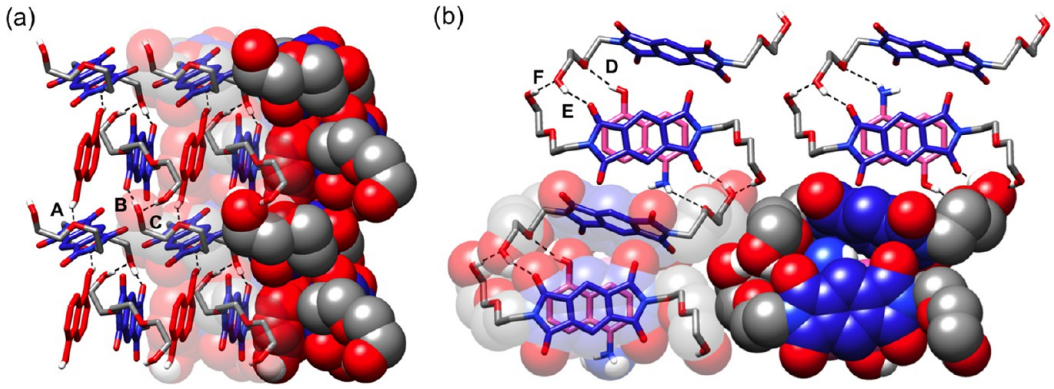

Figure 4. A blend of tubular and space-filling representations of the solid-state superstructures of isostructural LASO cocrystals (a) $(\mathbf{1}_A)_2{\cdot}\mathbf{7}_D$ viewed from the side of the mixed stacks and (b) $(\mathbf{1}_A)_2{\cdot}\mathbf{8}_D$ viewed along the face-to-face $\pi-\pi$ stacking direction. Hydrogen bonds are depicted as black dashed lines. (a) Cocrystal $(\mathbf{1}_A)_2{\cdot}\mathbf{7}_D$ incorporates bifurcated [O···O] hydrogen bonds between the edge-to-face $\mathbf{1}_A$ carbonyl groups and the mixed-stack $\mathbf{7}_D$ hydroxyl groups, as well as between the $\mathbf{1}_A$ DEG arms and the mixed-stack $\mathbf{7}_D$ hydroxyl groups and the $\mathbf{1}_A$ DEG arms to hold the stacks together, with distances of (A) 2.81, (B) 2.76, and (C) 2.79 Å, respectively. (b) A very similar hydrogen-bonded network can be appreciated with the aid of a blend of tubular and space-filling representations of the solid-state superstructure associated with the cocrystal $(\mathbf{1}_A)_2{\cdot}\mathbf{8}_D$, displaying bifurcated [N···O] and [O···O] hydrogen bonds between the edge-to-face $\mathbf{1}_A$ carbonyl groups and the mixed-stack $\mathbf{8}_D$ amino/hydroxyl groups, as well as between the $\mathbf{1}_A$ DEG arms and the mixed-stack $\mathbf{8}_D$ amino/hydroxyl groups and the $\mathbf{1}_A$ DEG arms, to hold the stacks together, with distances of (D) 2.88, (E) 2.79, and (F) 2.79 Å. Aromatic and alkyl H atoms not participating in hydrogen-bonding interactions shown in this illustration are omitted for the sake of clarity. Color code: $\mathbf{1}_A$ aromatic core, medium blue; $\mathbf{7}_D$ aromatic core, red; $\mathbf{8}_D$ aromatic core, pink; C, gray; H, white; O, red; N, blue.

$\pi-\pi$ interplanar distance of 3.33 Å. In contrast to $\mathbf{2}_A{\cdot}\mathbf{11}_D$, $\mathbf{2}_A{\cdot}\mathbf{9}_D$ contains intrastack hydrogen-bonding interactions between the $\mathbf{2}_A$ carbonyl groups and $\mathbf{9}_D$ amino functions, as well as [C−H···O] interactions between $\mathbf{9}_D$ and the $\mathbf{2}_A$ DEG arms ([N···O] distance 3.17 Å; [C···O] distance 3.40 Å). As expected, different CT stacks in the lattice interact through hydrogen bonds between the $\mathbf{2}_A$ carbonyl groups and the $\mathbf{9}_D$ amino functions and DEG arms in neighboring stacks, such that the stacks are arranged in a staggered fashion ([N···O] distance 3.49 Å; [O···O] distance 2.82 Å).

LASO Cocrystals in Group 2. Although donors $\mathbf{7}_D-\mathbf{9}_D$ are naphthalene derivatives with similar constitutions, the minor differences in the functional groups (NH_2 versus OH) lead to dramatic differences in the resulting packing and optical properties of the cocrystals. While cocrystal $\mathbf{1}_A{\cdot}\mathbf{9}_D$ consists of one-dimensional mixed stacks with equal amounts of donors and acceptors, the cocrystallizations of $\mathbf{1}_A$ with both $\mathbf{7}_D$ and $\mathbf{8}_D$ lead (Figure 4) to two isostructural cocrystals—$(\mathbf{1}_A)_2{\cdot}\mathbf{7}_D$ and $(\mathbf{1}_A)_2{\cdot}\mathbf{8}_D$—which consist of two symmetrically nonequivalent acceptors and one donor component. Both crystallize in the triclinic space group $P\bar{1}$ and contain two halves of the acceptor and one-half of the donor components in their asymmetric units. The PmI acceptors in the $(\mathbf{1}_A)_2{\cdot}\mathbf{7}_D$ cocrystals are organized (i) not only in a face-to-face fashion with the naphthalene donors along the [100] direction, wherein the D and A components are separated by 3.39 Å, (ii) but also in an edge-to-face manner along the [010] direction. This second CT interaction is stabilized by means of [C−H···π] interactions between the naphthalene protons of the face-to-face mixed stack and the $\mathbf{1}_A$ PmI aromatic cores of the second CT component ([H···π] distance 2.85 Å), such that the second component is tilted away from the stacking direction of the mixed stack by 61° with respect to the plane of the aromatic core of each component. As in the one-dimensional LASO superstructures, an extensive hydrogen-bonding network is also present in the cocrystal, holding the three components together in a tight manner. A number of [C−H···O] hydrogen bonds are present between the hydroxyl groups of $\mathbf{7}_D$ with the DEG arms of both $\mathbf{1}_A$ acceptor components ([C···O] distances 2.76 and 2.79 Å), as well as between the DEG arms of both $\mathbf{1}_A$ conformational isomers ([C···O] distance 2.81 Å). As a result of this hydrogen-bond network, stacks of the D−A cocrystals are enveloped by chains of $\mathbf{1}_A$ molecules that are formed through weak complementary [C−H···O] interactions between their carbonyl groups and aromatic protons ([C···O] distance 3.16 Å). Very similar interactions and long-range packing are observed for $(\mathbf{1}_A)_2{\cdot}\mathbf{8}_D$, where the mixed-stack core is separated by $\pi-\pi$ interplanar distances of 2.86 Å. This cocrystalline stack interacts through [C−H···π] interactions between the naphthalene protons and the second PmI conformational isomer ([H···π] distance 2.86 Å). As a result of the constitutionally unsymmetrical nature of $\mathbf{8}_D$, the positions of the OH and NH_2 groups are disordered across one of two possible orientations throughout the lattice. A hydrogen-bonding network is also formed that is similar to that of $(\mathbf{1}_A)_2{\cdot}\mathbf{7}_D$, in which cocrystalline mixed stacks are encased by the second PmI conformational isomer involving a series of [C−H···O] hydrogen bonds ([C···O] distances 2.88, 2.79, and 3.35 Å).

While the one-dimensional CT mixed stacks of group 1 exhibit[18] strong absorbance of linearly polarized light oriented parallel to the CT axis, the absorption spectra of cocrystals $(\mathbf{1}_A)_2{\cdot}\mathbf{7}_D$ and $(\mathbf{1}_A)_2{\cdot}\mathbf{8}_D$ are much more complex. Both absorb (Figure 5) light preferentially along two directions in the (001) plane. The strongest absorption bands (476 and 490 nm in the case of $(\mathbf{1}_A)_2{\cdot}\mathbf{7}_D$ and $(\mathbf{1}_A)_2{\cdot}\mathbf{8}_D$, respectively) can be attributed to the CT interactions between face-to-face D−A complexes along the [100] direction, while the second absorption bands (530 and 595 nm in the case of $(\mathbf{1}_A)_2{\cdot}\mathbf{7}_D$ and $(\mathbf{1}_A)_2{\cdot}\mathbf{8}_D$, respectively) are oriented 42 and 29° from the [100] direction, respectively. The absorption spectra of the two chromophores within these two cocrystals suggest that acceptors in both the face-to-face and edge-to-face directions participate in CT interactions. In each cocrystal, the polarization angles associated with the two electronic transitions are neither parallel nor perpendicular to each other. They are a consequence of strong anomalous dispersion across the visible spectrum, coupled with the fact that the triclinic crystals have no fixed eigendirections at any wavelength. Moreover, since the axes of refraction and absorption ellipsoids are never parallel to each other, additional

dx.doi.org/10.1021/ja509442t | J. Am. Chem. Soc. 2014, 136, 17224−17235

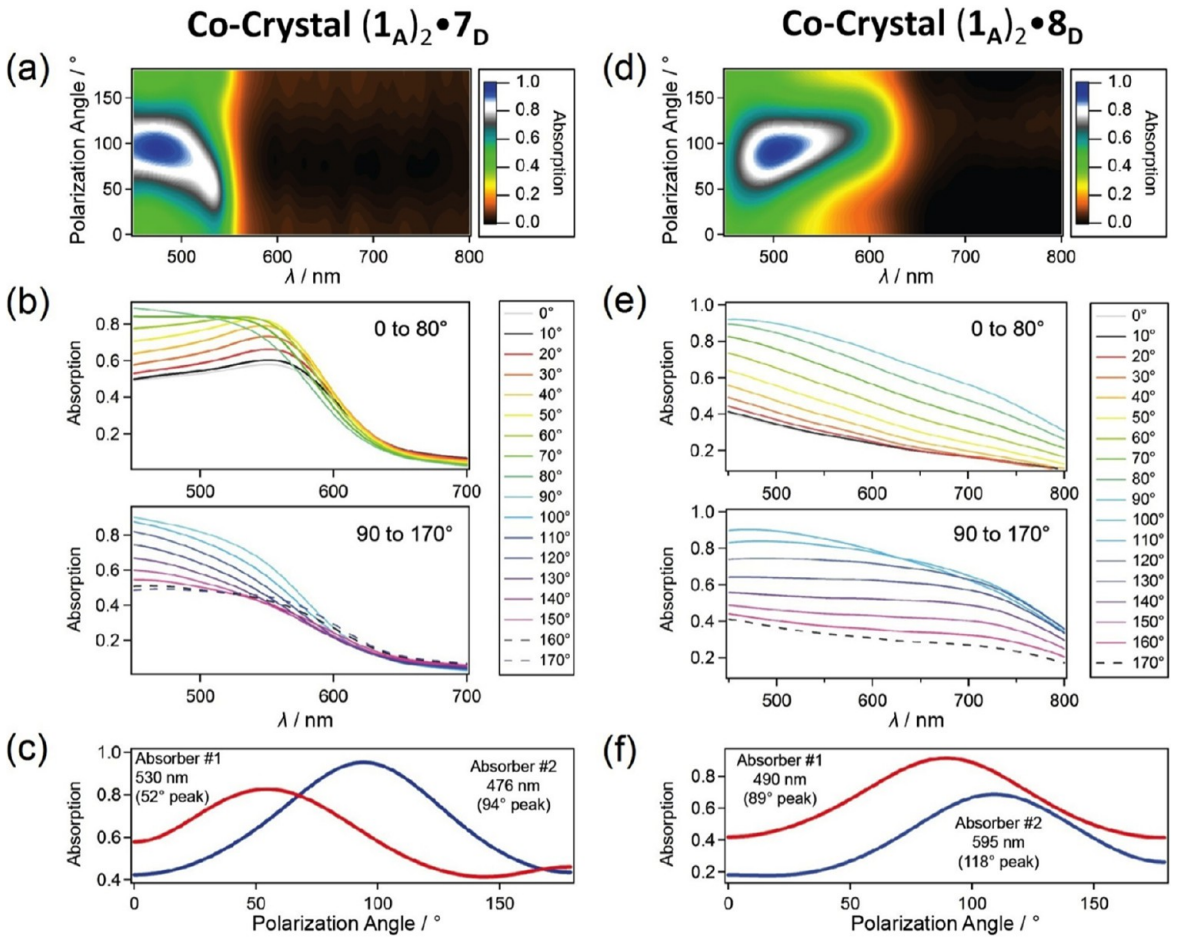

Figure 5. Polarized UV−visible spectra of (a, c) cocrystal $(1_A)_2$•7_D and (d, f) cocrystal $(1_A)_2$•8_D, revealing the presence of two distinct absorbance peaks arising from different CT pairs within the crossed-stack structure. The absorption spectra of the cocrystals $(1_A)_2$•7_D and $(1_A)_2$•8_D in (b) and (e) were measured every 10° from 0 to 80° (upper frames) and from 90 to 170° (lower frames).

ellipticities which couple the electronic absorptions may arise, even during linearly polarized illumination.[30] The bidirectional CT in the cocrystals leads (Figure 6) to pleochroism[31,32] in polarized light—that is, the color of the cocrystal changes with the polarization angle of incident white light. With the addition of a second polarizer (analyzer), crossed with respect to the first one, both cocrystals $(1_A)_2$•7_D and $(1_A)_2$•8_D fail to extinguish (Figure 6) when rotated in the path of incident white light. The crystals are bright at all orientations, and the colors transmitted vary across the visible spectrum.

LASO Cocrystals in Group 3. The long flexible DEG arms and functional groups participating in hydrogen bonding can also be located on the donor molecular components of LASO cocrystals. In this case, acceptors PmI 3_A and TCNQ 4_A are commercially available, and the naphthalene donors 5_D[33] and 6_D,[34] carrying DEG arms, can be synthesized readily before being combined to give rise to further CT cocrystals, demonstrating the modularity of the LASO design.

Two good examples (Figure 7) are the CT cocrystals 4_A•6_D and 3_A•5_D, containing donor components functionalized with the DEG arms. The 1,5-diaminonaphthalene derivative 6_D and the TCNQ acceptor 4_A cocrystallized (Figure 7a) in the triclinic space group $P\bar{1}$, with half a donor and half an acceptor molecule present in the asymmetric unit, while forming alternating D−A stacks with $\pi-\pi$ interplanar distances of 3.45 Å. The nitrile groups on 4_A do not participate[33] in significant hydrogen-bonding interactions. While there are no intrastack hydrogen-bonding interactions, a variety of interstack [N−H···O] and [O−H···O] hydrogen bonds are present between the DEG arms of neighboring 6_D molecules. These interactions hold the mixed stacks together in a staggered array ([O···O] distance 2.93 Å; [N···O] distance 3.02 Å). The naphthalene-based donor 5_D with DEG arms can be cocrystallized with 3_A under different liquid−liquid diffusion conditions to yield two crystalline morphologies. The cocrystal 3_A•5_D (Figure 7b), obtained by diffusing H_2O into a *N*-methylpyrrolidone (NMP) solution containing the D−A components, contains half a donor and half an acceptor molecule in the asymmetric unit and is identical with the crystal structure reported in the monoclinic space group $P2_1/c$ by Hamilton et al.[36,37] The D−A mixed stacks, in which the D and A components are separated by 3.32 Å, also contain intrastack [N−H···O] hydrogen bonds between the imide protons in 3_A and the DEG arms in 5_D ([N···O] distance 2.85 Å). The one-dimensional stacks are further bundled together in a herringbone fashion by interstack [C−H···O] hydrogen bonds between the DEG arms of 5_D molecules ([C···O] distances 2.85 and 2.78 Å). When aqueous Me_2SO cocrystallization conditions were employed, a solvate containing two Me_2SO molecules per D−A pair in the lattice was obtained. This solvate crystallized in the monoclinic space group $C2/c$ and contains half a donor, half an acceptor, and one solvent molecule in its asymmetric unit. The superstructure of 3_A•5_D•2Me_2SO, which does not qualify as a

dx.doi.org/10.1021/ja509442t | J. Am. Chem. Soc. 2014, 136, 17224−17235

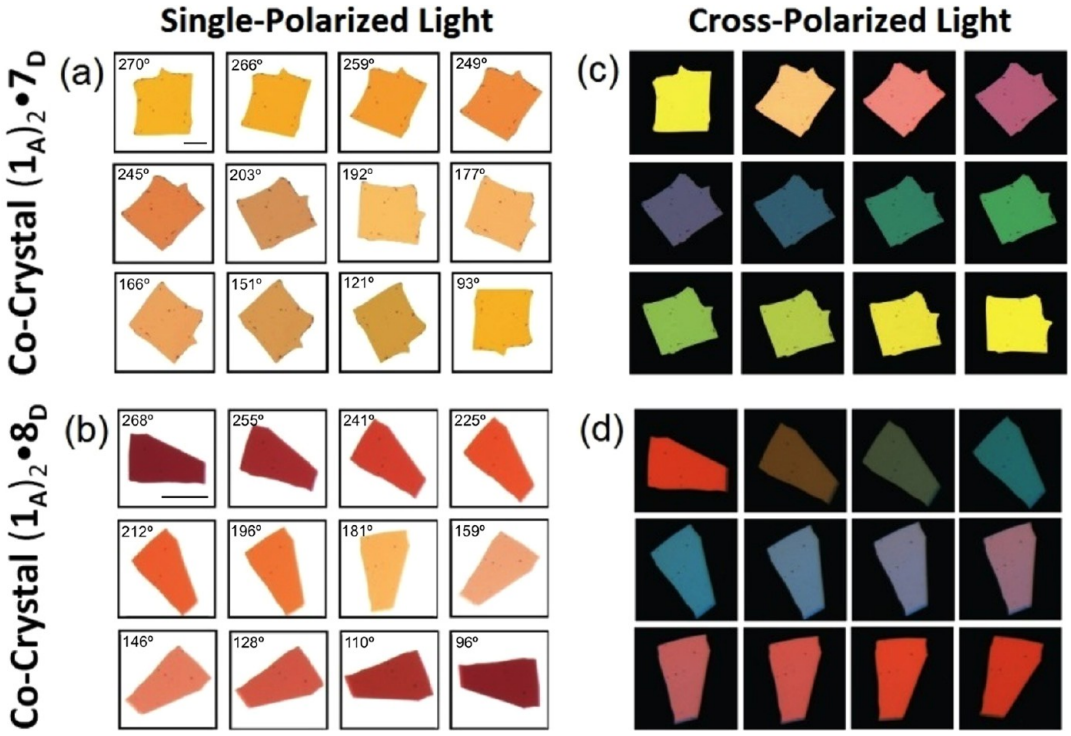

Figure 6. Images of single cocrystals $(\mathbf{1}_A)_2$•$\mathbf{7}_D$ and $(\mathbf{1}_A)_2$•$\mathbf{8}_D$ in (a, b) single-polarized mode and (c, d) cross-polarized mode. Cocrystals $(\mathbf{1}_A)_2$•$\mathbf{7}_D$ and $(\mathbf{1}_A)_2$•$\mathbf{8}_D$ exhibit bidirectional CT and consequence strong pleochroism with nonorthogonal absorption maxima that are a result of strong anomalous dispersion across the visible part of the electromagnetic spectrum in low-symmetry (triclinic) crystals. The scale bars (a, b) correspond to 50 μm for each crystal used in these experiments.

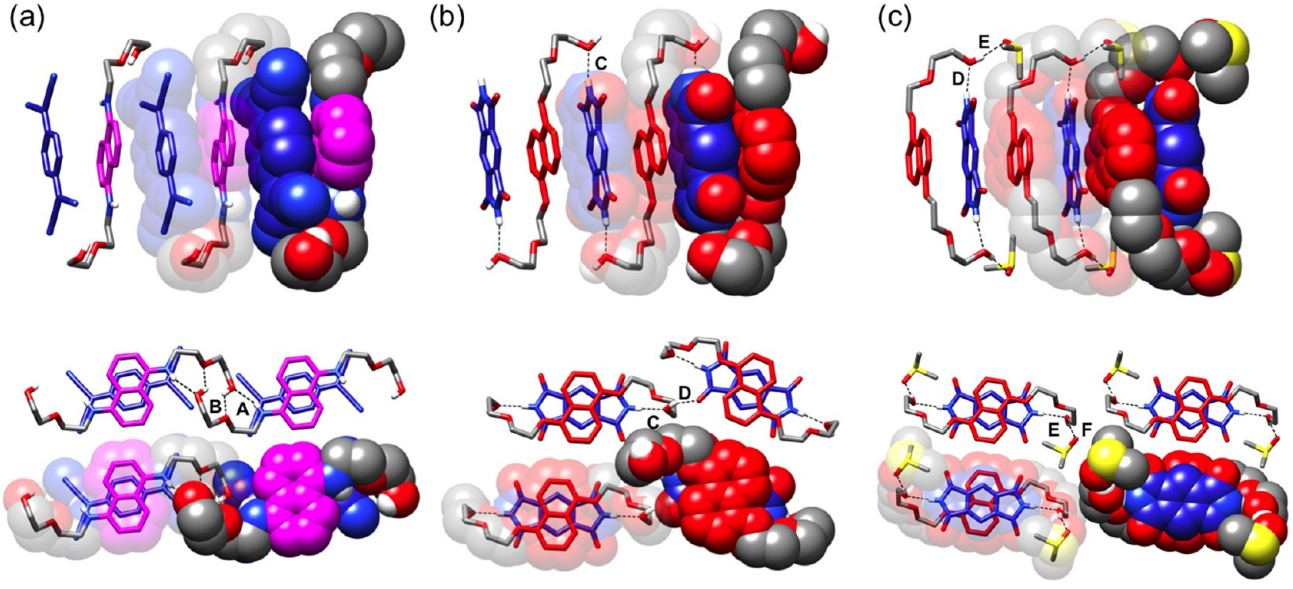

Figure 7. Blend of tubular and space-filling representations of the solid-state superstructures of LASO cocrystals (a) $\mathbf{4}_A$•$\mathbf{6}_D$ (b) $\mathbf{3}_A$•$\mathbf{5}_D$ and cocrystal (c) $\mathbf{3}_A$•$\mathbf{5}_D$•2Me_2SO viewed from both the side of the mixed stacks and along the CT π–π stacking directions, respectively. Hydrogen bonds are depicted by black dashed lines. (a) The mixed stacks of $\mathbf{4}_A$•$\mathbf{6}_D$ are held together by a series of [N···O] and [O···O] hydrogen bonds with distances of (A) 3.02 and (B) 2.93 Å, respectively. (b) A concerted series of bifurcated hydrogen bonds are observed in cocrystal $\mathbf{3}_A$•$\mathbf{5}_D$ between the $\mathbf{3}_A$ imide protons with the hydroxyl group $\mathbf{5}_D$ DEG arms of the same costack. The same $\mathbf{5}_D$ DEG protons interact with the carbonyl groups of neighboring costacks. The [N···O] and [O···O] hydrogen-bond distances observed are (C) 2.85 and (D) 2.78 Å, respectively. (c) Cocrystal $\mathbf{3}_A$•$\mathbf{5}_D$•2Me_2SO contains a series of [N···O] hydrogen bonds between the $\mathbf{3}_A$ DEG arms with both of the imide protons of a single $\mathbf{5}_D$ component, such that dimers are formed. Each of these DEG arms also participates in bifurcated [O···O] hydrogen bonds with Me_2SO solvent molecules at each side of the costack. The hydrogen-bond distances observed are (E) 2.92 and (F) 2.73 Å, respectively. Aromatic and alkyl H atoms not participating in hydrogen-bonding interactions shown in this illustration are omitted for the sake of clarity. Color code: $\mathbf{3}_A$ PmI and $\mathbf{4}_A$ TCNQ cores, medium blue; $\mathbf{5}_D$ and $\mathbf{6}_D$ naphthalene core, red and magenta; C, gray; H, white; O, red; N, blue.

dx.doi.org/10.1021/ja509442t | J. Am. Chem. Soc. 2014, 136, 17224–17235

Table 1. Liquid–Liquid Diffusion Cocrystallization Conditions of LASO Complexes

cocrystal	"bad" solvent	"good" solvent(s) (v/v)	concn[a] (mg/mL)	molar ratio (D:A)	growth time (days)
$\mathbf{1_A{\cdot}9_D}$	1-chlorobutane	dichloroethane/Et_2O (200/1)	2	2	3
$\mathbf{1_A{\cdot}10_D}$	1-chlorobutane	dichloroethane/Et_2O (20/1)	1.5	2	3
$\mathbf{1_A{\cdot}12_D}$	1-chlorobutane	dichloroethane/Et_2O (10/1)	1	2	3
$\mathbf{1_A{\cdot}7_D}$	1-chlorobutane	dichloroethane/Et_2O (10/1)	1.5	2	3
$\mathbf{1_A{\cdot}8_D}$	1-chlorobutane	dichloroethane/Et_2O (10/1)	1.5	2	3
$\mathbf{2_A{\cdot}9_D}$	1-chlorobutane	dichloroethane/Et_2O (20/1)	2	15[b]	3
$\mathbf{2_A{\cdot}11_D}$	1-chlorobutane	dichloroethane/Et_2O (20/1)	1	2	3
$\mathbf{3_A{\cdot}5_D}$	H_2O	*N*-methylpyrrolidone	2	1	5
$\mathbf{3_A{\cdot}5_D}{\cdot}2Me_2SO$	H_2O	dimethyl sulfoxide	2	1	5
$\mathbf{4_A{\cdot}6_D}$	1-chlorobutane	dichloroethane/Et_2O (10/1)	2	2	3

[a]The concentration refers to the electron acceptor in the crystallizing solution, not the total concentration of both constituents. [b]An excess of of $\mathbf{9_D}$ (15 equiv) was required to initiate cocrystallization due to solubility issues.

LASO cocrystal, draws attention to the importance of the choice of the solvent in LASO cocrystal growth. In the $\mathbf{3_A{\cdot}5_D}{\cdot}2Me_2SO$ mixed stacks, the alternating donor and acceptor components are found to be 3.37 Å apart. As expected, intrastack [N–H···O] bifurcated hydrogen-bonding interactions are present between the $\mathbf{3_A}$ amino functions and the $\mathbf{5_D}$ DEG arms ([N···O] distances 2.92 and 2.98 Å). In contrast with the examples of LASO cocrystals described previously, however, the DEG arms on $\mathbf{5_D}$ are both pointing toward the same molecule of $\mathbf{3_A}$, forming stacks of dimers rather than toward two different molecules in order to afford infinite LASO stacks. Furthermore, the importance of LASO cocrystals being free of solvent molecules is demonstrated in $\mathbf{3_A{\cdot}5_D}{\cdot}2Me_2SO$, in which the stacks are held together in an offset array through [O–H···O] hydrogen bonds between the $\mathbf{5_D}$ DEG arms and dimers of Me_2SO that are held together by [S···O] interactions, such that channels of solvent molecules are formed ([O···O] distance 2.73 Å; [S···O] distance 3.15 Å): i.e., the formation of the all-important LASO interstack hydrogen bonds are disrupted by the presence of solvent molecules.

CONCLUSIONS

The groundwork has been laid for the design and syntheses of a series of organic charge transfer cocrystals based on an innovative approach, namely the lock-arm supramolecular ordering (LASO) strategy, which consists of three components that work cooperatively to promote the multicomponent self-assembly processes. The components consist of (i) *complementary electron-rich and -deficient aromatic cores that form alternating donor–acceptor stacks*, (ii) *complementary hydrogen-bonding recognition units on the aromatic cores which form intermolecular hydrogen bonds*, and the use of (iii) *solvent systems which promote the rapid and solvent-free cocrystallization of the individual components*. The combination of charge transfer interactions and structurally flexible hydrogen-bonding motifs has been shown to constitute a good and reliable recipe for producing charge transfer cocrystals that can grow up to several centimeters in length under ambient conditions, often in no more than a few hours. We believe that this highly modular LASO protocol can serve as a general guide to crystal engineering,[6] since the donor–acceptor complexes lead to mixed-stack crystalline materials that are (i) fast growing, (ii) large in size, and (iii) stable both in and out of solution—a combination of attributes which has been observed only infrequently in other charge transfer cocrystalline arrays. Although a limited number (12) of building blocks have been investigated and LASO-derived cocrystals (9) have been realized, the concept of a molecular construction set extends[38] as far as our imagination allows. These features of the LASO design offer the possibility for the derived organic materials to acquire important functions in real-world applications related to a strong response to light or external fields.

EXPERIMENTAL SECTION

Cocrystallization Methods. Compounds $\mathbf{3_A}$, $\mathbf{4_A}$, and $\mathbf{7_D}$, $\mathbf{8_D}$, $\mathbf{9_D}$, $\mathbf{10_D}$ and $\mathbf{11_D}$ were obtained from commercial vendors, and compounds $\mathbf{1_A}$,[3] $\mathbf{2_A}$,[28] $\mathbf{5_D}$,[33] $\mathbf{6_D}$,[34] and $\mathbf{12_D}$[27] were prepared according to reported procedures. All 10 LASO CT cocrystals were grown under ambient conditions using a liquid–liquid diffusion protocol. Two distinct solvent protocols were found to promote expedient crystal growth: they were (i) the diffusion of anhydrous 1-chlorobutane into a D–A mixture in anhydrous 1,2-dichloroethane and Et_2O, and (ii) the diffusion of deionized H_2O into a D–A mixture in NMP. In order to ensure anhydrous crystallization condition, all glassware was dried in an oven or by using a heat gun while solvents were dried over alumina. All solvents and solutions were passed through PTFE syringe filters (0.45 μm) prior to layering. Detailed crystallization conditions, including the molar concentrations, ratios of solvent mixtures employed and times for crystal growth for the specific cocrystals discussed here are summarized in Table 1.

X-ray Crystallography. X-ray diffraction data were obtained on Bruker Platform and Kappa diffractometers, equipped with a MoKα or CuKα sealed-tube source and an APEX II CCD detector. Intensity data were collected using ω and φ scans spanning at least a hemisphere of reciprocal space for all structures (data were integrated using SAINT). Absorption effects were corrected on the basis of multiple equivalent reflections (SADABS). Structures were solved by direct methods[39] (SHELXS) and refined by full-matrix least squares against F^2 (SHELX). The structures were solved and refined using Olex2. Hydrogen atoms were assigned using riding isotropic displacement parameters and constrained to idealized geometries, including those bound to oxygen, as no hydrogen atoms could be located in the difference Fourier map.

Crystallographic Data. The crystallographic information and the structural parameters for the nine LASO cocrystals reported are given below.

$\mathbf{1_A{\cdot}9_D}$: $C_{56}H_{60}N_8O_{16}$; red needle, 0.664 × 0.107 × 0.046 mm^3; triclinic, space group $P\bar{1}$; a = 9.5063(4), b = 12.1715(6), c = 12.8872(6) Å; α = 61.896(3), β = 89.095(3), γ = 76.689(3)°; V = 1272.50(11) Å^3; Z = 1; ρ_{calcd} = 1.437 g cm^{-3}; $2\theta_{max}$ = 28.341°; T = 84(2) K; 6240 reflections collected, 4462 independent, 382 parameters; μ = 0.107 mm^{-1}; R_1 = 0.0533 [$I > 2.0\sigma(I)$], wR_2 = 0.1468 (all data); CCDC deposition number 988310.

$\mathbf{1_A{\cdot}10_D}$: $C_{34}H_{32}N_4O_8$; yellow needle, 0.534 × 0.164 × 0.074 mm^3; monoclinic, space group $P2_1/n$; a = 6.9937(2), b = 11.8675(2), c = 17.5154(3) Å; $\alpha = \gamma = 90$, β = 100.8960(10)°; V = 1427.53(5) Å^3; Z = 2; ρ_{calcd} = 1.453 g cm^{-3}; $2\theta_{max}$ = 67.21°; T = 100(2) K; 2479 reflections collected, 2290 independent, 220 parameters; μ = 0.869 mm^{-1}; R_1 = 0.0541 [$I > 2.0\sigma(I)$], wR_2 = 0.1497 (all data); CCDC deposition number 988305.

$\mathbf{1_A{\cdot}12_D}$: $C_{26}H_{28}N_2O_{10}S_4$; green needle, 0.666 × 0.11 × 0.081 mm^3; monoclinic, space group $P2_1/n$; a = 11.9236(4), b = 6.9553(3), c = 16.7123(5) Å; $\alpha = \gamma = 90$, β = 104.157(2)°; V = 1343.89(8) Å^3; Z = 2; ρ_{calcd} = 1.623 g cm^{-3}; $2\theta_{max}$ = 64.686°; T = 85(2) K; 2162 reflections collected, 1939 independent, 206 parameters; μ = 3.813 mm^{-1};

dx.doi.org/10.1021/ja509442t | J. Am. Chem. Soc. 2014, 136, 17224–17235

R_1 = 0.0439 [$I > 2.0\sigma(I)$], wR_2 = 0.1224 (all data); CCDC deposition number 988306.

2_A·9_D: $C_{32}H_{32}N_4O_8$; green needle, 0.457 × 0.119 × 0.012 mm^3; triclinic, space group $P\bar{1}$; a = 6.9510(2), b = 8.6966(2), c = 12.1281(3) Å; α = 72.093(2), β = 76.054(2), γ = 80.941(2)°; V = 674.30(3) Å^3; Z = 1; ρ_{calcd} = 1.479 g cm^{-3}; $2\theta_{max}$ = 30.062°; T = 100(2) K; 3880 reflections collected, 2073 independent, 285 parameters; μ = 0.108 mm^{-1}; R_1 = 0.0773 [$I > 2.0\sigma(I)$], wR_2 = 0.2540 (all data); CCDC deposition number 988309.

2_A·11_D: $C_{38}H_{33}N_3O_8$; green needle, 0.664 × 0.144 × 0.074 mm^3; triclinic, space group $P\bar{1}$; a = 10.9811(8), b = 12.4287(8), c = 12.9441(9) Å; α = 94.620(5), β = 112.518(5), γ = 109.840(5)°; V = 1489.33(19) Å^3; Z = 2; ρ_{calcd} = 1.471 g cm^{-3}; $2\theta_{max}$ = 64.856°; T = 85(2) K; 4883 reflections collected, 3438 independent, 466 parameters; μ = 0.858 mm^{-1}; R_1 = 0.0587 [$I > 2.0\sigma(I)$], wR_2 = 0.1798 (all data); CCDC deposition number 988308.

$(1_A)_2$·7_D: $C_{46}H_{48}N_4O_{18}$; red plate, 0.365 × 0.27 × 0.042 mm^3; triclinic, space group $P\bar{1}$; a = 6.78680(10), b = 10.8904(2), c = 15.7778(2) Å; α = 70.8800(10), β = 81.5540(10), γ = 83.1560(10)°; V = 1086.72(3) Å^3; Z = 1; ρ_{calcd} = 1.444 g cm^{-3}; $2\theta_{max}$ = 29.992°; T = 100(2) K; 6214 reflections collected, 4132 independent, 319 parameters; μ = 0.1112 mm^{-1}; R_1 = 0.0536 [$I > 2.0\sigma(I)$], wR_2 = 0.1346 (all data); CCDC deposition number 986213.

$(1_A)_2$·8_D: $C_{46}H_{49}N_5O_{17}$; red plate, 0.722 × 0.238 × 0.094 mm^3; triclinic, space group $P\bar{1}$; a = 6.7603(7), b = 10.8522(11), c = 15.785(2) Å; α = 71.882(9), β = 81.810(9), γ = 84.105(8)°; V = 1087.3(2) Å^3; Z = 1; ρ_{calcd} = 1.441 g cm^{-3}; $2\theta_{max}$ = 59.131°; T = 84(2) K; 3058 reflections collected, 2259 independent, 305 parameters; μ = 0.938 mm^{-1}; R_1 = 0.0568 [$I > 2.0\sigma(I)$], wR_2 = 0.1692 (all data); CCDC deposition number 986214.

4_A·6_D: $C_{30}H_{30}N_6O_4$; yellow block, 0.553 × 0.195 × 0.144 mm^3; triclinic, space group $P\bar{1}$; a = 6.8961(2), b = 8.0293(3), c = 12.3435(4) Å; α = 89.2130(10), β = 83.730(2), γ = 73.487(2)°; V = 651.25(4) Å^3; Z = 1; ρ_{calcd} = 1.373 g cm^{-3}; $2\theta_{max}$ = 67.174°; T = 100(2) K; 2233 reflections collected, 2173 independent, 189 parameters; μ = 0.763 mm^{-1}; R_1 = 0.0314 [$I > 2.0\sigma(I)$], wR_2 = 0.0838 (all data); CCDC deposition number 988304.

3_A·5_D: $C_{28}H_{28}N_2O_{10}$; yellow needle, 0.67 × 0.074 × 0.036 mm^3; monoclinic, space group $P2_1/c$; a = 6.6667(3), b = 23.3906(10), c = 8.3455(3) Å; $\alpha = \gamma$ = 90, β = 104.657(3)°; V = 1259.03(9) Å^3; Z = 2; ρ_{calcd} = 1.457 g cm^{-3}; $2\theta_{max}$ = 29.405°; T = 84(2) K; 3450 reflections collected, 2208 independent, 181 parameters; μ = 0.112 mm^{-1}; R_1 = 0.0653 [$I > 2.0\sigma(I)$], wR_2 = 0.1763 (all data); CCDC deposition number 988307.

3_A·5_D·2Me_2SO. $C_{32}H_{40}N_2O_{12}S_2$; yellow needle, 0.43 × 0.10 × 0.07 mm^3; monoclinic, space group $C2/c$; a = 32.625(3), b = 6.6459(7), c = 15.0606(15) Å; $\alpha = \gamma$ = 90, β = 95.288(6)°; V = 3251.6(6) Å^3; Z = 4; ρ_{calcd} = 1.448 g cm^{-3}; $2\theta_{max}$ = 30.07°; T = 100(2) K; 4771 reflections collected, 3838 independent, 224 parameters; μ = 0.232 mm^{-1}; R_1 = 0.0397 [$I > 2.0\sigma(I)$], wR_2 = 0.1145 (all data); CCDC deposition number 988312.

Comparison of Centrosymmetric and Non-centrosymmetric Crystallographic Solutions. It is evident that, when the structural data of the centrosymmetric superstructures are compared (Table 2−5) with their non-centrosymmetric refinements, that a centrosymmetric space group is the more appropriate crystallographic choice.[25] This situation is particularly evident when looking at the absolute configuration (Flack parameter) of the non-centrosymmetric structures. Furthermore, a number of structural parameters are flagged as serious inconsistencies with what would be expected from the data set by CheckCIF (http://checkcif.iucr.org/), all of which arise from missing symmetry elements in the structures, as well as, in the case of a number of the structures, the inability of the refinements to converge in a non-centrosymmetric space group.

UV−Visible Absorption Spectra. Absorption spectra were recorded using a polarizing microscope. A Nikon TE2000 inverted microscope and Prior ProScan II stage were employed to manipulate the sample position. The microscope halogen lamp was used as the source for the absorption spectra. Spectra were recorded using an Ocean Optics USB 2000 miniature spectrometer. The CT axes in the crystals

Table 2. Comparison of Centrosymmetric and Non-centrosymmetric Solutions of Group 1 LASO Cocrystals 1_A·9_D, 1_A·10_D, and 1_A·12_D

	1_A·9_D		1_A·10_D		1_A·12_D	
	non-centrosymmetric	centrosymmetric	non-centrosymmetric	centrosymmetric	non-centrosymmetric	centrosymmetric
space group	*P*1	$P\bar{1}$	*Pn*	$P2_1/n$	*P*1	$P\bar{1}$
R_1 [$I > 2.0\sigma(I)$]	0.2219	0.0533	0.0484	0.0541	0.0810	0.0587
wR_2	0.5357	0.1318	0.1354	0.01463	0.2185	0.1605
no. of restraints	326	0	3	0	888	0
Flack param	−0.5(10)		0.3(4)		−0.5(6)	
CIF check alert	structural refinement does not converge; ADDSYM suggests $P\bar{1}$ is correct space group (100% fit); abnormal bond lengths and angles; low bond precision	none	ADDSYM suggests $P2_1/n$ is correct space group (100% fit); abnormal hydrogen bond lengths	none	structural refinement does not converge; ADDSYM suggests $P\bar{1}$ is correct space group (97% fit); abnormal hydrogen bond lengths; low bond precision	none
param correlation (%)	>58	<73	>77	<50	>72	<63

dx.doi.org/10.1021/ja509442t | J. Am. Chem. Soc. 2014, 136, 17224−17235

Table 3. Comparison of Centrosymmetric and Non-centrosymmetric Solutions of Group 1 LASO Cocrystals $2_A{\cdot}9_D$ and $2_A{\cdot}11_D$

	$2_A{\cdot}9_D$		$2_A{\cdot}11_D$	
	non-centrosymmetric	centrosymmetric	centrosymmetric	non-centrosymmetric
space group	$P1$	$P\bar{1}$	$P2_1/n$	$P2_1$
R_1 $[I > 2.0\sigma(I)]$	0.2219	0.0773	0.0483	0.0447
wR_2	0.5357	0.2129	0.1187	0.1217
no. of restraints	326	153	1	9
Flack param	−0.5(10)			−0.11(5)
CIF check alert	structural refinement does not converge; ADDSYM suggests $P\bar{1}$ is correct space group (100% fit); abnormal bond lengths and angles; low bond precision	none	none	ADDSYM suggests $P2_1/n$ is correct space group (100% fit); abnormal hydrogen bond lengths
param correlation (%)	>58	<74	<50	>86

Table 4. Comparison of Centrosymmetric and Non-centrosymmetric Solutions of Group 2 LASO Cocrystals $(1_A)_2{\cdot}7_D$ and $(1_A)_2{\cdot}8_D$

	$(1_A)_2{\cdot}7_D$		$(1_A)_2{\cdot}8_D$	
	non-centrosymmetric	centrosymmetric	non-centrosymmetric	centrosymmetric
space group	$P1$	$P\bar{1}$	$P1$	$P\bar{1}$
R_1 $[I > 2.0\sigma(I)]$	0.0518	0.0542	0.0507	0.0568
wR_2	0.1103	0.1219	0.1268	0.1528
no. of restraints	3	0	162	0
Flack param	−1 (2)		−0.3 (0.6)	
CIF check alert	ADDSYM suggests $P\bar{1}$ is correct space group (100% fit); bad thermal params; low C−C bond precision; abnormal bond lengths	none	ADDSYM suggests $P\bar{1}$ is correct space group (100% fit); bad thermal params; low C−C bond precision; abnormal bond lengths; poor data/param ratio	none
param correlation (%)	>90	<50	>88	<59

Table 5. Comparison of Centrosymmetric and Non-centrosymmetric Solutions of Group 3 LASO Cocrystals $4_A{\cdot}6_D$ and $3_A{\cdot}5_D$

	$4_A{\cdot}6_D$		$3_A{\cdot}5_D$	
	non-centrosymmetric	centrosymmetric	non-centrosymmetric	centrosymmetric
space group	$P1$	$P\bar{1}$	Pc	$P2_1/c$
R_1 $[I > 2.0\sigma(I)]$ (%)	3.06	3.14	5.88	6.53
wR_2 (%)	8.83	8.32	11.53	15.22
no. of restraints	3	0	361	0
Flack param	0.4 (2)		−7.6 (10)	
CIF check alert	ADDSYM suggests $P\bar{1}$ is correct space group (100% fit)	none	ADDSYM suggests $P2_1/c$ is correct space group (100% fit); bad thermal params; low bond precision	none
param correlation (%)	>83	<50	>90	<59

were identified initially by performing solid-state 2D polarized UV−visible spectroscopy on single crystals of $(1_A)_2{\cdot}7_D$ and $(1_A)_2{\cdot}8_D$. The crystals were rotated through 180° and the relative angles of maximum absorbance indexed. The crystallographic axes were then identified on an X-ray diffractometer and related to the relative polarization angles obtained previously during the solid-state UV−visible spectroscopic measurements. The dichroic ratios at the absorption maxima of the two chromophores in the complexes $(1_A)_2{\cdot}7_D$ and $(1_A)_2{\cdot}8_D$ were found to differ significantly, thereby verifying the presence of two chromophores.

Optical Measurements. Pleochroism measurements were performed on cocrystals by capturing a portion of the transmitted light using an Ocean Optics SD2000 CCD detector. Each 2D plot was corrected for high-frequency CCD detector and background noise by subtracting the light transmitted through the polarizers in the absence of the cocrystal.

■ ASSOCIATED CONTENT

Supporting Information

CIF files giving crystallographic data for all X-ray structure determinations in this paper. This material is available free of charge via the Internet at http://pubs.acs.org.

■ AUTHOR INFORMATION

Corresponding Authors

*E-mail for S.I.S.: s-stupp@northwestern.edu
*E-mail for J.F.S.: stoddart@northwestern.edu

Author Contributions

#These authors contributed equally.

Notes

The authors declare no competing financial interest.

■ ACKNOWLEDGMENTS

We thank Dr. Amy A. Sarjeant, Charlotte L. Stern, and the personnel in the Integrated Molecular Structure Education and Research Center (IMSERC) at Northwestern University (NU) for their assistance in the collection of X-ray crystallographic data. Molecular crystal images were produced using the UCSF Chimera package from the Resource for Biocomputing, Visualization, and Informatics at the University of California, San Francisco. The research conducted in the Stoddart laboratory is part (Project 34-949) of the Joint Center of Excellence in Integrated Nano-Systems (JCIN) at King

Abdulaziz City for Science and Technology (KACST) and NU. The authors thank both KACST and NU for their continued support of this research. The work performed in the Stupp laboratory was supported by a grant from the U.S. Department of Energy, Basic Energy Sciences (DE-FG02-00ER45810). The contributions of B.K. were supported by the NSF (DMR-1105000). A.K.B. acknowledges Fulbright New Zealand for a Fulbright Graduate Award and the New Zealand Federation of Graduate Women for a Postgraduate Fellowship Award. D.C., who was supported by an NSF Graduate Research Fellowship, also acknowledges support from a Ryan Fellowship awarded by the NU International Institute for Nanotechnology (IIN). R.W. acknowledges a JSPS Postdoctoral Fellowship for Research Abroad.

REFERENCES

(1) (a) Lehn, J.-M. *Supramolecular Chemistry*; Wiley-VCH: Weinheim, Germany, 1995. (b) Stoddart, J. F. *Nat. Chem.* **2009**, *1*, 14.

(2) Eliel, E. L. *Science and Serendipity: The Importance of Basic Research*; American Chemical Society: Washington, DC, 1992.

(3) Tayi, A. S.; Shveyd, A. K.; Sue, A. C.-H.; Szarko, J. M.; Rolczynski, B. S.; Cao, D.; Kennedy, T. J.; Sarjeant, A. A.; Stern, C. L.; Paxton, W. F.; Wu, W.; Dey, S. K.; Fahrenbach, A. C.; Guest, J. R.; Mohseni, H.; Chen, L. X.; Wang, K. L.; Stoddart, J. F.; Stupp, S. I. *Nature* **2012**, *488*, 485.

(4) (a) Stupp, S. I.; LeBonheur, V.; Walker, K.; Li, L. S.; Huggins, K. E.; Keser, M.; Amstutz, A. *Science* **1997**, *276*, 384. (b) Brunsveld, L.; Folmer, B. J. B.; Meijer, E. W.; Sijbesma, R. P. *Chem. Rev.* **2001**, *101*, 4071. (c) Stoddart, J. F.; Colquhoun, H. M. *Tetrahedron* **2008**, *64*, 8231. (d) Aida, T.; Meijer, E. W.; Stupp, S. I. *Science* **2012**, *335*, 813.

(5) (a) Ludlow, R. F.; Otto, S. *Chem. Soc. Rev.* **2008**, *37*, 101. (b) Nitschke, J. R. *Nature* **2009**, *462*, 736. (c) Gibb, B. C. *Nat. Chem.* **2009**, *1*, 252. (d) Gibb, B. C. *Nat. Chem.* **2011**, *3*, 3. (e) Otto, S. *Acc. Chem. Res.* **2012**, *45*, 2200. (f) Stoddart, J. F. *Angew. Chem., Int. Ed.* **2012**, *51*, 12902. (g) Lehn, J.-M. *Angew. Chem., Int. Ed.* **2013**, *52*, 2836.

(6) (a) Desiraju, G. R. *Crystal Engineering. The Design of Organic Solids*; Elsevier: Amsterdam, 1989. (b) Desiraju, G. R. *Angew. Chem., Int. Ed. Engl.* **1995**, *34*, 2311.

(7) (a) Smaldone, R. A.; Forgan, R. S.; Furukawa, H.; Gassensmith, J. J.; Slawin, A. M. Z.; Yaghi, O. M.; Stoddart, J. F. *Angew. Chem., Int. Ed.* **2010**, *49*, 8630. (b) Gassensmith, J. J.; Furukawa, H.; Smaldone, R. A.; Forgan, R. S.; Botros, Y. Y.; Yaghi, O. M.; Stoddart, J. F. *J. Am. Chem. Soc.* **2011**, *133*, 15312. (c) Forgan, R. S.; Smaldone, R. A.; Gassensmith, J. J.; Furukawa, H.; Cordes, D. B.; Li, Q.; Wilmer, C. E.; Botros, Y. Y.; Snurr, R. Q.; Slawin, A. M. Z.; Stoddart, J. F. *J. Am. Chem. Soc.* **2012**, *134*, 406. (d) Liu, Z.; Frasconi, M.; Lei, J.; Brown, Z. J.; Zhu, Z.; Cao, D.; Iehl, J.; Liu, G.; Fahrenbach, A. C.; Farha, O. K.; Hupp, J. T.; Mirkin, C. A.; Botros, Y. Y.; Stoddart, J. F. *Nat. Commun.* **2013**, *4*, 1855. (e) Gassensmith, J. J.; Jeong, N. C.; Kim, J. Y.; Farha, O. K.; Stoddart, J. F.; Hupp, J. T. *J. Am. Chem. Soc.* **2014**, *136*, 8277.

(8) (a) Saunder, D. H. *Proc. R. Soc. London, Ser. A* **1946**, *188*, 31. (b) Vanniekerk, J. N.; Saunder, D. H. *Acta Crystallogr.* **1948**, *1*, 44. (c) Andrews, L. J. *Chem. Rev.* **1954**, *54*, 713. (d) McConnell, H. *J. Chem. Phys.* **1954**, *22*, 760. (e) Desantis, F.; Liquori, A. M.; Giglio, E.; Ripamonti, A. *Nature* **1961**, *191*, 900. (f) McConnell, H. M.; Hoffman, B. M.; Metzger, R. M. *Proc. Natl. Acad. Sci. U.S.A.* **1965**, *53*, 46. (g) Kuroda, H.; Ikemoto, I.; Akamatu, H. *Bull. Chem. Soc. Jpn.* **1966**, *39*, 5471. (h) Foster, R. *Organic Charge-Transfer Complexes*; Academic Press: New York, 1969. (i) Mayerle, J. J.; Torrance, J. B.; Crowley, J. I. *Acta Crystallogr., Sect. B* **1979**, *B35*, 2988. (j) Hunter, C. A.; Sanders, J. K. M. *J. Am. Chem. Soc.* **1990**, *112*, 5525. (k) Hunter, C. A.; Lawson, K. R.; Perkins, J.; Urch, C. J. *J. Chem. Soc., Perkin Trans. 2* **2001**, 651. (l) Waters, M. L. *Curr. Opin. Chem. Biol.* **2002**, *6*, 736.

(9) (a) Herbstein, F. H. *Crystalline Molecular Complexes and Compounds: Structures and Principles*; Oxford University Press: Oxford, U.K., 2005. (b) Klosterman, J. K.; Yamauchi, Y.; Fujita, M. *Chem. Soc. Rev.* **2009**, *38*, 1714.

(10) (a) Jérome, D.; Schulz, H. J. *Adv. Phys.* **2002**, *51*, 293. (b) Horiuchi, S.; Hasegawa, T.; Tokura, Y. *J. Phys. Soc. Jpn.* **2006**, *75*, 051016. (c) Saito, G.; Yoshida, Y. *Bull. Chem. Soc. Jpn.* **2007**, *80*, 1.

(11) Soos, Z. G. *Annu. Rev. Phys. Chem.* **1974**, *25*, 121.

(12) Anderson, P. W.; Lee, P. A.; Saitoh, M. *Solid State Commun.* **1973**, *13*, 595.

(13) (a) Torrance, J. B.; Girlando, A.; Mayerle, J. J.; Crowley, J. I.; Lee, V. Y.; Batail, P.; Laplaca, S. J. *Phys. Rev. Lett.* **1981**, *47*, 1747. (b) Girlando, A.; Pecile, C.; Torrance, J. B. *Solid State Commun.* **1985**, *54*, 753. (c) Iwasa, Y.; Koda, T.; Tokura, Y.; Kobayashi, A.; Iwasawa, N.; Saito, G. *Phys. Rev. B: Condens. Matter* **1990**, *42*, 2374. (d) Kuwata-Gonokami, M.; Peyghambarian, N.; Meissner, K.; Fluegel, B.; Sato, Y.; Ema, K.; Shimano, R.; Mazumdar, S.; Guo, F.; Tokihiro, T.; Ezaki, H.; Hanamura, E. *Nature* **1994**, *367*, 47.

(14) For a definition of the term coconformation, see: Fyfe, M. C. T.; Glink, P. T.; Menzer, S.; Stoddart, J. F.; White, A. J. P.; Williams, D. J. *Angew. Chem., Int. Ed. Engl.* **1997**, *36*, 2068.

(15) (a) Ferraris, J.; Cowan, D. O.; Walatka, V., Jr.; Perlstein, J. H. *J. Am. Chem. Soc.* **1973**, *95*, 948. (b) Coleman, L. B.; Cohen, M. J.; Sandman, D. J.; Yamagishi, F. G.; Garito, A. F.; Heeger, A. J. *Solid State Commun.* **1973**, *12*, 1125. (c) Jérome, D. *Chem. Rev.* **2004**, *104*, 5565.

(16) (a) Horiuchi, S.; Okimoto, Y.; Kumai, R.; Tokura, Y. *Science* **2003**, *299*, 229. (b) Collet, E.; Lemée-Cailleau, M. H.; Buron-Le Cointe, M.; Cailleau, H.; Wulff, M.; Luty, T.; Koshihara, S.-Y.; Meyer, M.; Toupet, L.; Rabiller, P.; Techert, S. *Science* **2003**, *300*, 612. (c) Kobayashi, K.; Horiuchi, S.; Kumai, R.; Kagawa, F.; Murakami, Y.; Tokura, Y. *Phys. Rev. Lett.* **2012**, *108*, 237601.

(17) Kagawa, F.; Horiuchi, S.; Tokunaga, M.; Fujioka, J.; Tokura, Y. *Nat. Phys.* **2010**, *6*, 169.

(18) (a) Tan, J. J.; Ma, Z.; Xu, W.; Zhao, G.; Geng, H.; Di, C.; Hu, W.; Shuai, Z.; Singh, K.; Zhu, D. *J. Am. Chem. Soc.* **2013**, *135*, 558. (b) Zhang, J.; Geng, H.; Virk, T. S.; Zhao, Y.; Tan, J.; Di, C. A.; Xu, W.; Singh, K.; Hu, W.; Shuai, Z.; Liu, Y.; Zhu, D. *Adv. Mater.* **2012**, *24*, 2603. (c) Park, S. K.; Varghese, S.; Kim, J. H.; Yoon, S.-J.; Kwon, O. K.; An, B.-K.; Gierschner, J.; Park, S. Y. *J. Am. Chem. Soc.* **2013**, *135*, 4757. (d) Sagade, A. A.; Rao, K. V.; George, S. J.; Datta, A.; Kulkarni, G. U. *Chem. Commun.* **2013**, *49*, 5847.

(19) (a) Hughes, R. C.; Soos, Z. G. *J. Chem. Phys.* **1968**, *48*, 1066. (b) Huizinga, S.; Kommandeur, J.; Sawatzky, G. A.; Thole, B. T.; Kopinga, K.; Dejonge, W. J. M.; Roos, J. *Phys. Rev. B: Condens. Matter* **1979**, *19*, 4723. (c) Soos, Z. G.; Keller, H. J.; Ludolf, K.; Queckbörner, J.; Wehe, D.; Flandrois, S. *J. Chem. Phys.* **1981**, *74*, 5287. (d) LePage, T. J.; Breslow, R. *J. Am. Chem. Soc.* **1987**, *109*, 6412. (e) Hasegawa, T.; Kagoshima, S.; Mochida, T.; Sugiura, S.; Iwasa, Y. *Solid State Commun.* **1997**, *103*, 489. (f) Enoki, T.; Miyazaki, A. *Chem. Rev.* **2004**, *104*, 5449.

(20) (a) Rao, S. M.; Batra, A. K.; Lal, R. B.; Evans, R. A.; Loo, B. H.; Metzger, R. M.; Lee, W. J. *J. Appl. Phys.* **1991**, *70*, 6674. (b) Ezaki, H.; Kuwata-Gonokami, M.; Shimano, R.; Ema, K.; Hanamura, E.; Fluegel, B.; Meissner, K.; Mazumdar, S.; Peyghambarian, N. *Solid State Commun.* **1993**, *88*, 211. (c) Mazumdar, S.; Guo, F.; Meissner, K.; Fluegel, B.; Peyghambarian, N.; Kuwata-Gonokami, M.; Sato, Y.; Ema, K.; Shimano, R.; Tokihiro, T.; Ezaki, H.; Hanamura, E. *J. Chem. Phys.* **1996**, *104*, 9283. (d) Wong, M. S.; Pan, F.; Gramlich, V.; Bosshard, C.; Gunter, P. *Adv. Mater.* **1997**, *9*, 554. (e) Zyss, J.; Ledoux-Rak, I.; Weiss, H. C.; Blaser, D.; Boese, R.; Thallapally, P. K.; Thalladi, V. R.; Desiraju, G. R. *Chem. Mater.* **2003**, *15*, 3063.

(21) For recent reviews, see: (a) Das, A.; Ghosh, S. *Angew. Chem., Int. Ed.* **2014**, *53*, 2038. (b) Mohit, K.; Rao, V. K.; George, S. J. *Phys. Chem. Chem. Phys.* **2014**, *16*, 1300.

(22) Gidden, J.; Wyttenbach, T.; Jackson, A. T.; Scrivens, J. H.; Bowers, M. T. *J. Am. Chem. Soc.* **2000**, *122*, 4692.

(23) (a) Kitagawa, S.; Kitaura, R.; Noro, S.-I. *Angew. Chem., Int. Ed.* **2004**, *43*, 2334. (b) Yamada, T.; Otsubo, K.; Makiurac, R.; Kitagawa, H. *Chem. Soc. Rev.* **2013**, *42*, 6655.

(24) (a) Eddaoudi, M.; Moler, D. B.; Li, H. L.; Chen, B. L.; Reineke, T. M.; O'Keeffe, M.; Yaghi, O. M. *Acc. Chem. Res.* **2001**, *34*, 319. (b) Yaghi, O. M.; O'Keeffe, M.; Ockwig, N. W.; Chae, H. K.; Eddaoudi, M.; Kim, J. *Nature* **2003**, *423*, 705. (c) Long, J. R.; Yaghi, O. M. *Chem. Soc. Rev.* **2009**, *38*, 1213.

(25) The superstructures of cocrystals $\mathbf{1}_A\cdot\mathbf{9}_D$, $\mathbf{1}_A\cdot\mathbf{10}_D$, and $\mathbf{1}_A\cdot\mathbf{12}_D$ were initially reported as existing in non-centrosymmetric space groups in ref 3. After further structural investigation, however, it was confirmed by X-ray crystallography that the structures can only be refined as being centrosymmetric. Despite carrying out a large number of X-ray diffraction experiments, we have been unable to establish the presence of non-centrosymmetry in the cocrystals $\mathbf{1}_A\cdot\mathbf{9}_D$, $\mathbf{1}_A\cdot\mathbf{10}_D$, and $\mathbf{1}_A\cdot\mathbf{12}_D$, a situation that is required in order to observe ferroelectric properties. In previously reported organic charge transfer cocrystals, it has been demonstrated (see refs 10 and 26) that the structural dimerization or distortion of donor and acceptor molecules can break lattice symmetry. Neutron diffraction experiments and theoretical calculations are currently underway to identify the reason for polarization in these particular cocrystals. These techniques may reveal small changes in the relative positions of the components and/or their electronic composition which could lead to non-centrosymmetry in the cocrystals.
(26) (a) Le Cointe, M.; Lemee-Cailleau, M. H.; Cailleau, H.; Toudic, B.; Toupet, L.; Heger, G.; Moussa, F.; Schweiss, P.; Kraft, K. H.; Karl, N. *Phys. Rev. B* **1995**, *51*, 3374. (b) García, P.; Dahaoui, S.; Katan, C.; Souhassou, M.; Lecomte, C. *Faraday Discuss.* **2007**, *135*, 217.
(27) Nozdryn, T.; Clemenceau, D.; Cousseau, J.; Morisson, V.; Gorgues, A.; Orduna, J.; Uriel, S.; Garín, J. *Synt. Met.* **1993**, *56*, 1768.
(28) Chen, S.; Zeng, X. C. *J. Am. Chem. Soc.* **2014**, *136*, 6428.
(29) Bevers, S.; Schutte, S.; McLaughlin, L. W. *J. Am. Chem. Soc.* **2000**, *122*, 5905.
(30) Claborn, K.; Chu, A.-S.; Jang, S.-H.; Su, F.; Kaminsky, W.; Kahr, B. *Cryst. Growth Des.* **2005**, *5*, 2117.
(31) Rogers, A. F.; Kerr, P. F. *Optical Mineralogy*; McGraw-Hill: New York, 1942.
(32) Kahr, B.; Gurney, R. W. *Chem. Rev.* **2001**, *101*, 893.
(33) Asakawa, M.; Dehaen, W.; Labbe, G.; Menzer, S.; Nouwen, J.; Raymo, F. M.; Stoddart, J. F.; Williams, D. J. *J. Org. Chem.* **1996**, *61*, 9591.
(34) Sue, C. H.; Basu, S.; Fahrenbach, A. C.; Shveyd, A. K.; Dey, S. K.; Botros, Y. Y.; Stoddart, J. F. *Chem. Sci.* **2010**, *1*, 119.
(35) Le Questel, J. Y.; Berthelot, M.; Laurence, C. J. *Phys. Org. Chem.* **2000**, *13*, 347.
(36) Hamilton, D. G.; Lynch, D. E.; Byriel, K. A.; Kennard, C. H. L. *Aust. J. Chem.* **1997**, *50*, 439.
(37) The cocrystal $\mathbf{3}_A\cdot\mathbf{5}_D$ was first reported (ref. 36) by Hamilton et al. The authors also concluded that the hydrogen-bonding array can be further extended to other supramolecular architectures.
(38) Cao, D.; Hong, M.; Blackburn, A. K.; Liu, Z.; Holcroft, J. M.; Stoddart, J. F. *Chem. Sci.* **2014**, *5*, 4242.
(39) Sheldrick, G. *Acta Crystallogr., Sect. A* **2008**, *64*, 112.